Application of the Saderholm Erosive Burning Model to Nozzleless Solid Propellant Rocket Motors

Clark D. Mikkelsen*
U.S. Army Missile Command, Redstone Arsenal, Alabama
and
G. Patrick Roys†
Morton-Thiokol, Huntsville, Alabama

This paper demonstrates the ability of the Saderholm erosive burning model, when coupled with the Air Force Rocket Propulsion Laboratory Nozzleless Rocket Motor Internal Ballistics Computer Program, to predict the ballistic performance of six nozzleless rocket motors of three designs loaded with three nonaluminized HTPB propellants. The paper describes the Saderholm erosive burning model, the six nozzleless test motors, and the ballistics prediction methodology. The results for instantaneous and total ballistic parameters show that the Saderholm erosive burning model as developed for nozzled rocket motors predicts the ballistic performance of nozzleless rocket motors as well as or better than the Erosive Model 1 developed specifically for nozzleless rocket motors and built into the AFRPL computer program.

Nomenclature

a = empirical constant
c = gas sonic velocity, m/s
G = mass flux parallel to the propellant surface, kg/s-m^2
G_0 = threshold value of mass flux, kg/s-m^2
m = empirical constant
M = local Mach number
M_c = critical Mach number
P = local static pressure, Pa
r = burn rate, m/s
r_m = burn rate in the motor, m/s
r_o = ballistic burn rate, m/s
R_H = hydraulic radius of the port, m
x = empirical constant

Introduction

IN an attempt to extend the current knowledge of erosive burning in solid propellant rocket motors, a study was conducted to demonstrate the ability of the Saderholm erosive burning model, when coupled with the Air Force Rocket Propulsion Laboratory (AFRPL) Nozzleless Rocket Motor Internal Ballistics Computer Program, to predict the ballistic performance of six nozzleless rocket motors of three designs loaded with three nonaluminized HTPB (hydroxy-terminated polybutadiene) propellants. This demonstration should be a crucial one for any erosive burning model, since nozzleless solid propellant rocket motors are known to exhibit a wide spectrum of erosive burning throughout the entire motor burn with port Mach numbers ranging from zero to supersonic values at any instant of time. Furthermore, none of the traditional erosive burning models for nozzled rocket motors have thus far been shown to give good ballistic predictions for nozzleless solid propellant rocket motors.

Submitted June 7, 1982; presented as Paper 82-1146 at the AIAA/SAE/ASME 18th Joint Propulsion Conference, Cleveland, Ohio, June 21-23, 1982; revision received July 18, 1983.

*Aerospace Engineer. Member AIAA.
†Principal Investigator, Engineering Department. Currently with Rockwell International, Atlanta, Ga.

Saderholm Erosive Burning Model

Propellant burning rate in a solid propellant rocket motor can be significantly different from that measured with small strands burning in a closed vessel at identical conditions of pressure and temperature. This phenomenon, usually called "erosive burning," is caused by the passage of combustion gases over the burning propellant surface.

One of the many theoretical and/or empirical models to account for this burn rate augmentation was developed by Saderholm,[1] who found erosive burning to be directly related to the fluid flow parameters regulating heat transfer to the propellant by forced convection. The empirical constants in the model were originally based on data taken with PBAA (polybutadiene-acrylic acid) aluminized propellant samples in a 0.03048 m diam blast tube, but has been extended to propellants having different binder systems and no aluminum.

Saderholm found that propellant burning could be described in three regimes, the nonerosive, transition, and full erosive regimes, which, for a given static pressure, are determined by the local Mach number (Fig. 1).

For high subsonic Mach numbers starting at about 0.5, the full erosive regime, the burn rate was independent of the ballistic burn rate and given by the equation.

$$r = 4.44599 \times 10^{-7} (MP)^{0.71}.$$

This correlation follows Anderson[2] and is based on a form of the Nusselt expression for the surface coefficient of forced convection developed for turbulent flow in pipes.

For Mach numbers less than about 0.06, the non-erosive regime, the burn rate was unaffected by the gas flow, i.e., the observed rate was equal to the ballistic burn rate.

Between Mach numbers of 0.06 and 0.5, a transition zone existed where burn rate was described by

$$r = r_o [M/M_c]^x$$

with the critical Mach number M_c corresponding to a velocity of 76.2 m/s below which erosive burning does not occur.

Figure 2 shows how the exponent x varied as a function of local static pressure and ballistic burn rate for the PBAA propellants used in Saderholm's original research. The transition region is assumed to end whenever the full erosive burn rate just exceeds that defined by the burn rate equation for the transition regime.

To correct for motors with port diameters other than 0.03048 m and noncircular propellant grains, Saderholm recommended a hydraulic radius correction factor given by

$$r_m = r[0.03048/4R_H]^{0.2}.$$

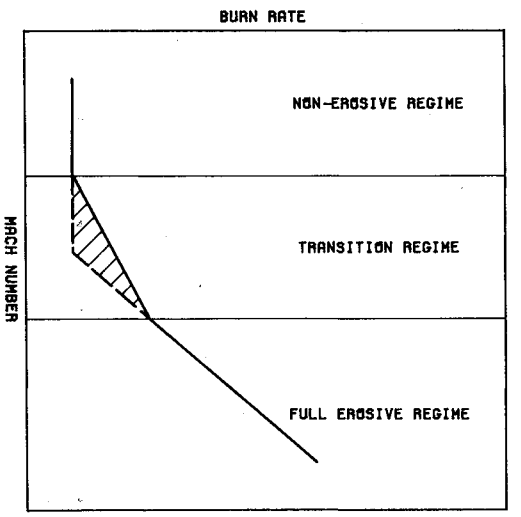

Fig. 1 Propellant burn rate as a function of Mach number at constant pressure.

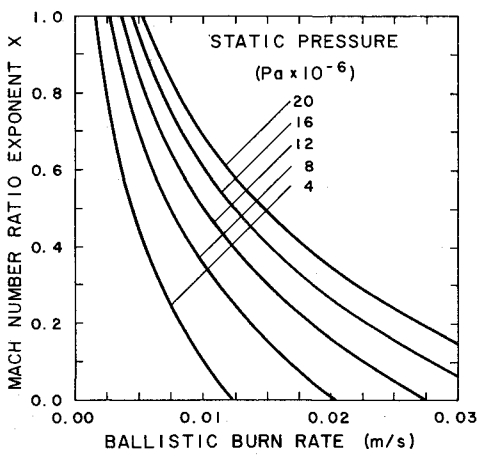

Fig. 2 Mach number ratio exponent.

AFRPL Computer Code and Erosive Burning Model

The AFRPL Nozzleless Rocket Motor Internal Ballistics Computer Program, the only computer program common to the propulsion industry for the prediction of the ballistic performance of nozzleless solid propellant rocket motors, was developed in 1973 and later revised in 1979. The computer model provides a transient, one-dimensional treatment of nozzleless motor ballistics; however, the method is approximate in that the time-dependent terms are retained only in the continuity equation. The computer program includes numerous options of various levels of sophistication to treat such details of motor operation as ignition transients and grain deflection, but only the most readily usable options were exercised in this study. The computer model is reported to give, in general, 3-4% accuracy in total impulse and 5-8% accuracy in head-end pressure and thrust with errors as large as 15% in peak ignition pressure.[3,4]

The revised version of the AFRPL Nozzleless Rocket Motor Internal Ballistics Computer Program contains options for three erosive burning models, including the traditional Lenoir-Robillard model; however, only the empirical model developed with the original computer program from nozzleless rocket motor static firing tests, and referred to here as the Erosive Burning Model 1, has been used widely. The Erosive Burning Model 1 gives the propellant burn rate as

$$r = r_o + a(G^m - G_o^m)\,[Ug/c]^{0.5}$$

The three constants G_o, a, and m are known to be highly dependent on the propellant formulation and motor conditioning temperature, although values of $G_o = 140.614$ kg/s-m^2, $a = 6.13171 \times 10^{-4}$, and $m = 0.095$ have been recommended for non-aluminized HTPB propellants and these values were used throughout this study.[4]

Motor and Propellant Descriptions

Static motor firing data measured in three different nozzleless rocket motors burning three propellants were used for the analyses reported herein. Major dimensions and propellant designations for these motors are listed in Table 1.

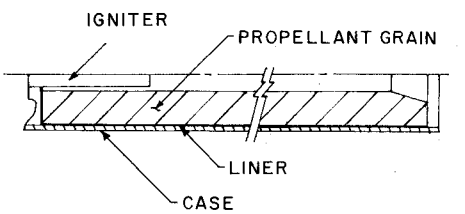

Fig. 3 TX715 motor assembly.

Table 1 Motor characteristics

Characteristic	Motor designation					
	TX715/T944-1	TX715/T943-1	TX669/T772-1	TX669/T762-1	TX665/T760-1	TX665/T761-1
Propellant designation	DTS-9336	DTS-9336	TP-H8254	DTS-8236	DTS-8236	DTS-8236
Motor temperature at static firing, K	335	218	293	293	293	293
Strand temperature, K	335	335	293	293	293	293
Grain i.d., n	0.040767	0.040767	0.027813	0.027813	0.027813	0.027813
Grain o.d., n	0.108204	0.108204	0.109220	0.109220	0.095834	0.095834
Grain length, n	1.203681	1.203681	1.192530	1.192530	1.303020	1.303020
Conical expansion half angle, rad	0.523599	0.523599	0.471239	0.471239	0.471239	0.471239
Mass of propellant burned, kg	17.22	17.19	17.21	16.92	13.45	13.34

One motor (designation TX715) was a flight-weight version of an air-to-air missile motor (Fig. 3). It featured a constant 0.1143 m o.d. case made of AISI 4130 steel having a nominal wall thickness of 0.001016 m.[5]

The second motor (TX669) was a test-weight version of an air-to-air missile motor (Fig. 4) very similar to the TX715 in overall configuration and sized to represent a 0.1143-m-diam motor. It featured a thick-wall steel case shaped to simulate a boat-tail at the aft end.[6]

The third motor (TX665) was a test-weight version of an air-to-ground missile motor (Fig. 5). In addition to being slightly smaller in diameter than the TX715 and TX669 motors (representing a 0.1016 m diameter), it featured a section at the aft end where the motor o.d. was reduced to provide space for flight controls.[7]

The propellant of all three motors was cast into cases lined with carbon-filled HTPB polymer, so that the propellant was bonded to the case during its cure cycle. All propellant grains had the same basic configuration of a constant diameter inner bore (slightly smaller in TX669 and TX665 motors) with a conical expansion section at the aft end. The boat-tail at the aft end of the TX669 produced a mechanical nozzling effect just prior to propellant burnout. As a result of the reduced diameter section of the TX665 design, this motor operated in the nozzleless mode only for approximately half of its total duration; thereafter it behaved as a nozzled motor (albeit an inefficient one) until all propellant was consumed. None of the propellant surfaces were inhibited, so that burning occurred on all unbonded surfaces.

Flat plate closures sealed the forward ends of the pressure vessels for all motors. The igniters were mounted in the forward closures and remained intact throughout motor operation. All igniters operated for approximately 0.1 s. There was essentially no free volume between the forward end of the propellant grain and the forward closure (the nominal separation being 0.001270 m) in the TX715 and TX665 motors; a nominal separation of 0.012700 m provided approximately 0.000115 m^3 of free volume in the TX669 motor.

The non-aluminized propellant in each motor was loaded from a 0.019 m^3 mix. Propellant characteristics are listed in Table 2. One formulation (designation DTS-9336) was loaded in the two TX715 motors, and another (DTS-9336) was loaded in the two TX665 motors. The TX669 motors each contained a different propellant (DTS-8236 and TP-H8254).

Ballistics Prediction Methodology

The ballistics prediction technique using the AFRPL Nozzleless Rocket Motor Internal Ballistics Computer Program was identical for each of the six nozzleless test motors, using either the Saderholm erosive burning model or Erosive Burning Model 1. Since motors TX665/T760-1 and TX665/T761-1 were duplicates, they were treated as a single motor for the computer prediction, and all static firing measurements required for the prediction, such as motor web time, were taken as an average value for the two motors.

Propellant grain geometry inputs for each motor were taken directly from the design drawings corresponding to Figs. 3-5. No allowance was made for geometric variations due to cure shrinkage, motor conditioning temperature, or grain deflection during motor operation.

Twenty-eight computational nodes were located from the head-end to aft-end of each motor in a nearly logarithmic distribution so as to concentrate nodes as the virtual throat (start of the conical expansion section) where gradients in the motor flowfield were expected to be highest.

Simulated motor ignition was accomplished in each prediction using the "Δt" option, which begins the internal ballistic calculations from the equilibrium condition associated with a given fast pressure rise time. The fast pressure rise time was input as the static firing measured value for each motor. No attempt was made to account for igniter mass addition.

Since all six of the nozzleless test motors were designed for head-end burning, that opinion in the AFRPL internal ballistics computer code was initiated at time zero assuming instantaneous ignition of the entire head-end propellant surface.

Only one value of the thermodynamic and transport properties, as calculated with the NASA Lewis thermochemistry computer program[8] at the time-averaged head-

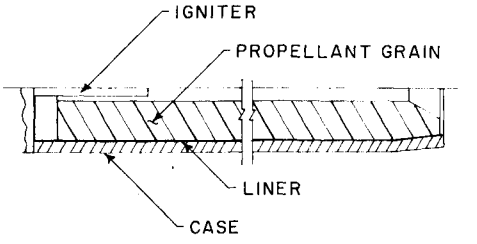

Fig. 4 TX669 motor assembly.

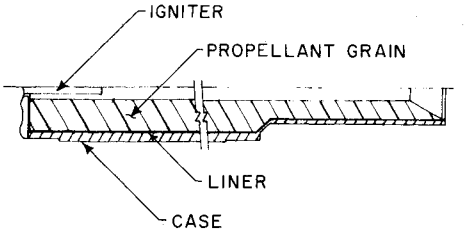

Fig. 5 TX665 motor assembly.

Table 2 Propellant characteristics

Characteristic	Propellant designation DTS-9336	DTS-8236	TP-H8254
Formulation			
Binder, HTPB[a]	12.3	12.0	13.5
Oxidizer, AP[b]	86.0	87.0	85.0
Combustion stabilizer, ZrC. C[c]	1.0/0.0	0.0/0.0	0.5/1.0
Burn rate catalyst, FEO[d]	0.7	1.0	0.0
Oxidizer size, $M \times 10^{-6}$	200/50/5	200/50/5	400/200/50
Oxidizer distribution, %	50/20/30	15/35/50	40/20/40
Burn rate m/s at 6.894×10^6 Pa and 293 K	0.021	0.021	0.015
Pressure exponent at 6.894×10^6 Pa and 293 K	0.5	0.4	0.4

[a]HTPB = Hydroxy-terminated polybutadiene. [b]AP = Ammonium perchlorate. [c]ZrC = Zirconium carbide, C = Carbon. [d]FEO = Ferric oxide

Table 3 Ballistic parameter summary

Ballistic parameter	Motor designation TX715/T944-1	TX715/T943-1	TX669/T772-1	TX669/T762-1	TX665/T760-1	TX665/T761-1	Erosive burning model
Ballistic burn rate scale factor for	1.02009	0.990000	1.16300	1.13000	1.16281	1.16281	S
matched web time	0.075950	0.838000	0.995000	0.985872	0.995000	0.995000	E
% Error in maximum	0.0	−3.232	−17.741	−15.234	−5.894	−2.308	S
head-end pressure	0.0	4.450	9.695	−3.656	10.136	13.179	E
% Error in	9.501	2.929	−15.758	−6.124	−3.510	−11.342	S
maximum thrust	8.799	4.837	16.778	3.553	12.291	5.654	E
% Error in mean	14.053	11.281	−2.634	−1.561	3.830	7.145	S
thrust to web time	6.974	3.305	−5.780	−7.185	4.151	7.455	E
% Error in mean	−0.682	−0.052	0.243	−1.173	2.177	3.333	S
specific impulse	−1.955	−2.475	−0.852	−2.476	2.925	4.073	E
% Error in	4.602	5.047	−3.709	−6.557	0.047	0.388	S
total impulse	3.395	2.748	−4.847	−7.930	0.812	1.150	E
% Error in impulse	7.029	4.810	−4.651	−5.065	0.040	1.150	S
to web time	3.753	−0.509	−7.448	−9.892	0.721	2.873	E

[a] S = Saderholm erosive burning model, E = Erosive Burning Model 1.

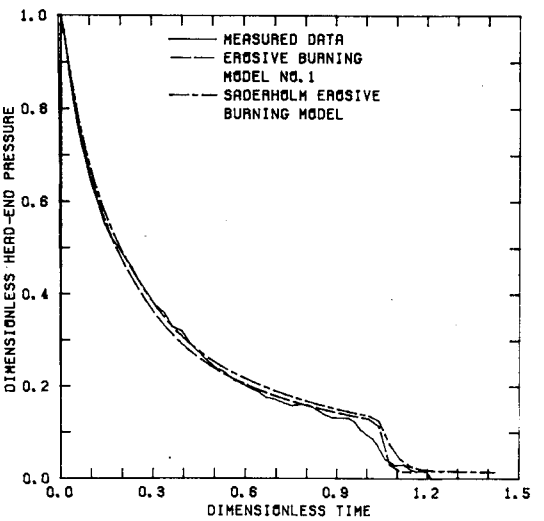

Fig. 6 TX715/T944-1 head-end pressure history.

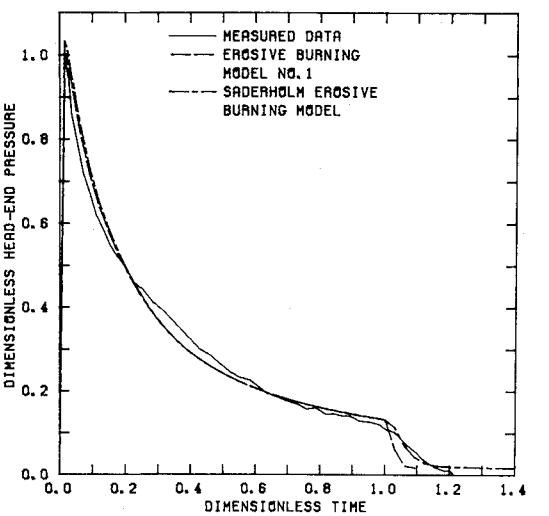

Fig. 8 TX715/T943-1 head-end pressure history.

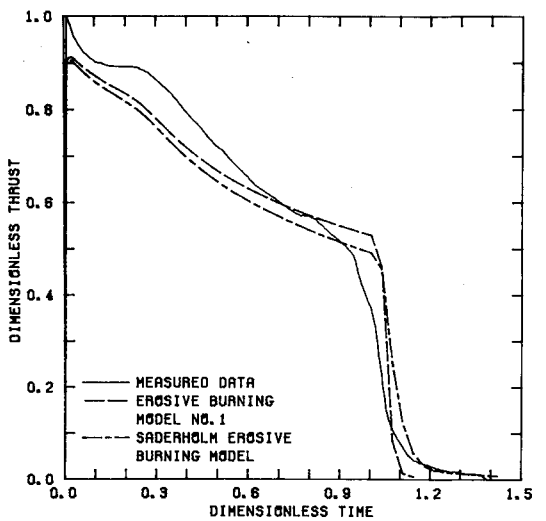

Fig. 7 TX715/T944-1 thrust history.

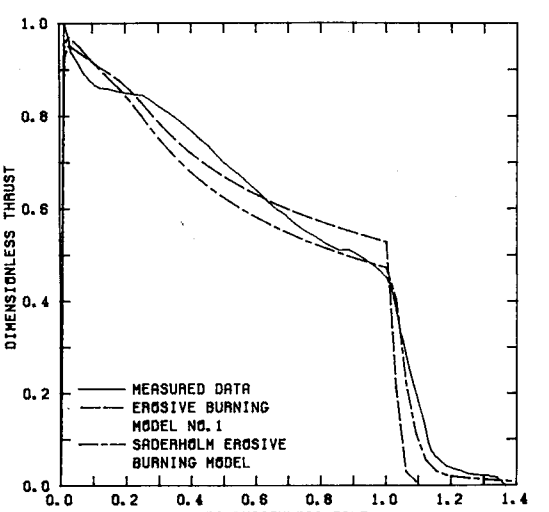

Fig. 9 TX715/T943-1 thrust history.

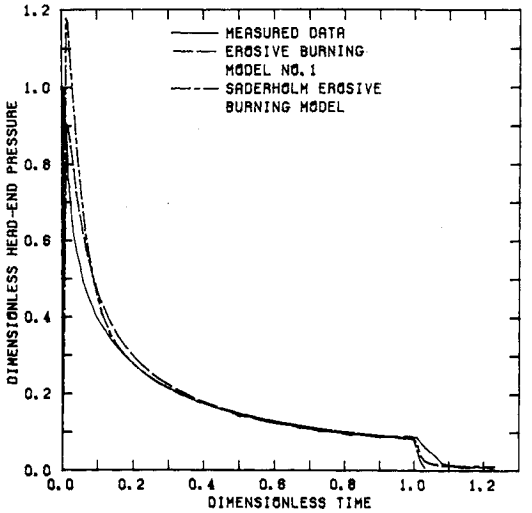

Fig. 10 TX669/T772-1 head-end pressure history.

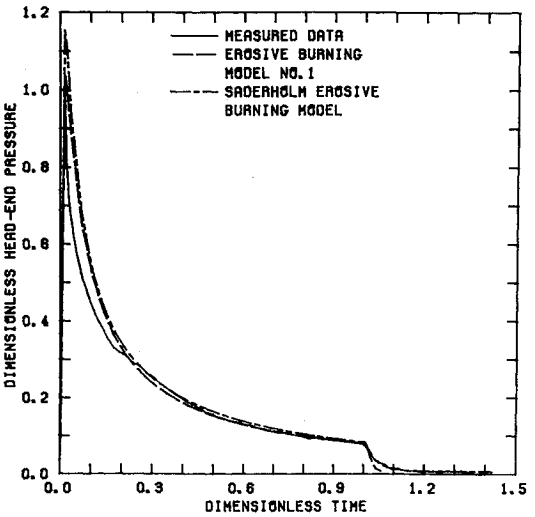

Fig. 12 TX669/T762-1 head-end pressure history.

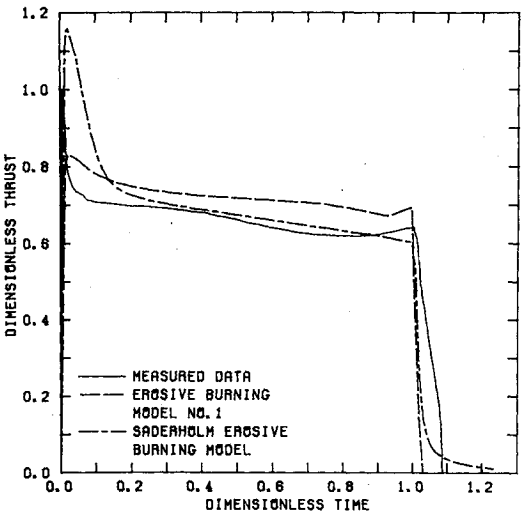

Fig. 11 TX669/T772-1 thrust history.

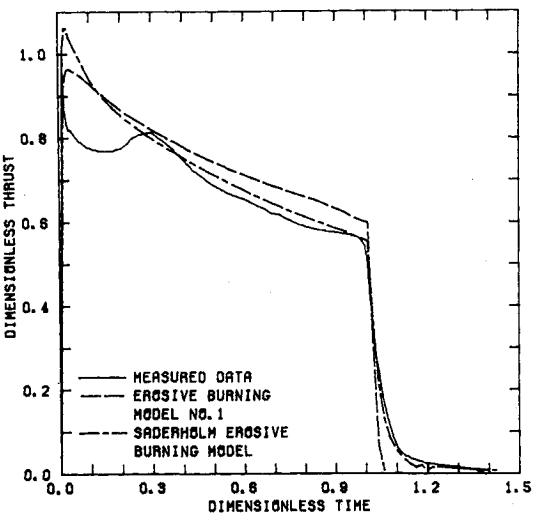

Fig. 13 TX669/T762-1 thrust history.

end pressure from static firing measurements, was input for each motor. In each case, the flame temperature was reduced to 95% of theoretical to account for combustion inefficiencies.

Ballistic burn rate data for each propellant were measured with cured strands; however, a scale factor was applied to this data for each motor and each erosive burning model such that the predicted motor web time, the time when the propellant web burns to the motor case, matched the static firing value. The scale factor for each prediction is listed in Table 3 with the ballistic parameter summary.

Results

Results of this study for each of the six nozzleless test motors are given in the head-end pressure and thrust histories of Figs. 6-15 with an error summary for select instantaneous and total ballistic parameters presented in Table 3. The pressure and thrust histories compare the computer predictions for both the Saderholm erosive burning model and Erosive Burning Model 1 with the static firing measurements. Measured values for head-end pressure and thrust for both motors TX665/T760-1 and TX665/T761-1 are shown in Figs. 14 and 15; the ballistic parameters are listed separately in Table 3 for these motors. Head-end pressure and thrust values in Figs. 6-15 were divided by the corresponding maximum measured value for the given motor to give dimensionless quantities. Similarly, time was divided by the given motor web time as determined from static firing data.

Examination of the head-end pressure and thrust histories of Figs. 6-15 reveals a number of qualitative observations of note. Both the Saderholm erosive burning model and the Erosive Burning Model 1 give better head-end pressure predictions than thrust predictions, which can be expected from a simple, one-dimensional internal ballistics computer model. Furthermore, the goodness of fit appears to run generally the same for both erosive burning models, either good or mediocre. The Saderholm erosive burning model does seem more capable of modeling a gradual tail-off process as occurs in Figs. 8 and 9, whereas tail-off is always abrupt using Erosive Burning Model 1. The best fit for both erosive burning models occurs for motors TX715/T944-1 and TX715/T943-1, even though these were fired at the temperature extremes of 335 K and 218 K, with the computer predictions run from the same set of strand burn rate data taken at 335 K initial temperature, as indicated in Table 1. The worst fit for both erosive burning models occurs for motors TX665/T760-1 and TX665/T761-1, and may be attributed to the restricted aft-end closure seen in Fig. 5, which changes the nozzleless motor operation to that of a nozzled motor as the aft portion of the grain is consumed.

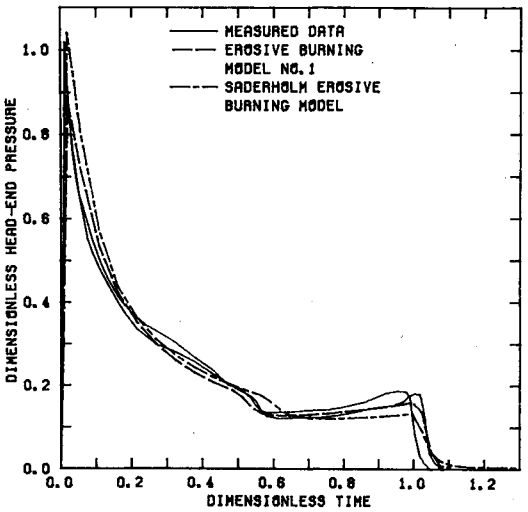

Fig. 14 TX665/T760-1 and TX665/T761-1 head-end pressure history.

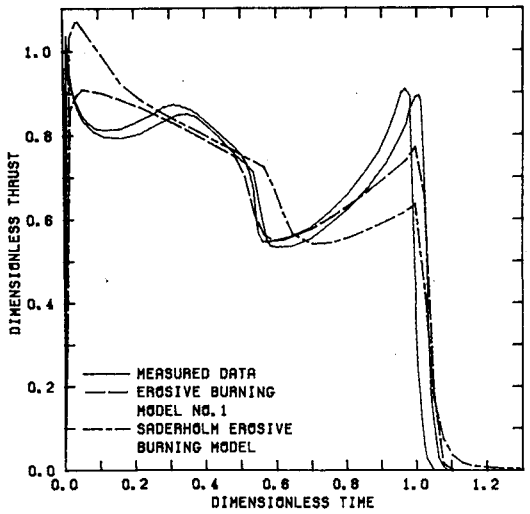

Fig. 15 TX665/T760-1 and TX665/T761-1 thrust history.

Significant trends can also be seen in the instantaneous and total ballistic parameters of Table 3. The ballistic burn rate scale factor was always less than unity for predictions using the Erosive Burning Model 1, and always greater than unity for predictions using the Saderholm erosive burning model, provided the motor and strands had the same conditioning temperature. The Saderholm erosive burning model is more likely to overpredict the maximum head-end pressure and thrust, whereas the Erosive Burning Model 1 is more likely to underperdict these quantities. Finally, and perhaps most importantly, the Saderholm erosive burning model gives consistently smaller errors in mean specific impulse than Erosive Burning Model 1. All of the errors in instantaneous and total ballistic parameters were of the same magnitude reported for the AFRPL Nozzleless Rocket Motor Internal Ballistics Computer Program.

Conclusions

The ballistic prediction methodology employed in this study is somewhat subjective. Certainly pre-test measurement for exact propellant grain dimensions and efforts to account for igniter mass flow and grain deflection may improve the ballistic predictions, although not necessarily to the same degree for the two erosive burning models. The addition of a broader class of nozzleless test motors to include aluminized propellants would generalize the study; however, the treatment of nozzleless motor ballistics with two-phase flows is much more complex and may add uncertainty to the results.

Furthermore, within the limitations of the ballistics prediction methodology and the AFRPL Nozzleless Rocket Motor Internal Ballistics Computer Program, it can be concluded that for these six nozzleless test motors the Saderholm erosive burning model, as originally developed for nozzled rocket motors, predicts the ballistic performance of nozzleless rocket motors as well as or better than the Erosive Burning Model 1 developed specifically for nozzleless rocket motors. These analyses also provide indirect confirmation that the Saderholm model describes erosive burning at Mach numbers greater than 0.5.

This is the first study to demonstrate the successful application of one of the traditional nozzled motor erosive burning model to nozzleless rocket motors.

This demonstration of the universality of the Saderholm model should promise future improvement in the ballistic prediction methodology for nozzleless rocket motors since the Saderholm model is not sensitive to motor temperature or, though not documented here, propellant formulation.

Acknowledgment

The authors wish to thank the Huntsville Division of Morton-Thiokol Corporation for permission to publish the paper, which was written while the authors were employed with the Huntsville Division.

References

[1]Saderholm, C. A., "A Characterization of Erosive Burning for Composite H-Series Propellants," AIAA Solid Propellant Rocket Conference, Palo Alto, Calif., Jan. 1964.

[2]Anderson, S. E., "A Discussion of the Parameters Affecting the Burning Rate of Hybrid Fuels," Rohm & Haas Co., Redstone Arsenal Research Division, Huntsville, Ala., Second ARPA Hybrid Meeting, Jan. 1963.

[3]Harry, D. P., Price, C. F., Small, K. R., and Taylor, D. E., "Nozzleless Rocket Motor Internal Ballistics Computer Program Development," AFRPL-TR-73-19, March 1973.

[4]Clement, J. A., Harry, D. P., Markle, R. J., Procinsky, I. M., and Smith, W. R., "Revised User's Manual for the Nozzleless Rocket Motor Internal Ballistics Computer Program," AFRPL-TR-78-82, March 1979.

[5]Roys, G. P., et al., "Low Cost Missile Motor Demonstration Program," AFRPL-TR-80-65, Nov. 1980.

[6]Maser, D. D., Hessler, R. O., and Roys, G. P., "Comparison of LCLM Nozzleless Rocket Motors with Two Propellants," Thiokol/Huntsville Division, Huntsville, Ala., Rept. RER-944, June 1977.

[7]Maser, D. D., Hessler, R. O., and Roys, G. P., "Nozzleless Advanced Tactical Rocket Motor Test and Analysis," Thiokol/Huntsville Division, Huntsville, Ala., Rept. RER-943, June 1977.

[8]Svehla, R. A. and McBride, B. J., "FORTRAN IV Computer Program for Calculation of Thermodynamic and Transport Properties of Complex Chemical Systems," NASA TND-7056, Jan. 1973.